J Sol-Gel Sci Technol (2015) 74:783–789
DOI 10.1007/s10971-015-3663-y

ORIGINAL PAPER

Sol–gel synthesis of α-Fe_2O_3 nanoparticles and its photocatalytic application

M. Alagiri · Sharifah Bee Abdul Hamid

Received: 25 October 2014 / Accepted: 10 February 2015 / Published online: 17 February 2015

Abstract α-Fe_2O_3 nanoparticles was synthesized through a simple and efficient sol–gel process using citric acid and triethanolamine. The phase structure, morphology, and optical properties of the as-prepared products were extensively characterized by X-ray diffraction, scanning electron microscopy, Raman spectroscopy, and ultraviolet spectroscopy. The chemical compositions of the as-synthesized α-Fe_2O_3 nanoparticles have been analyzed by Fourier transform infrared spectroscopy. X-ray diffraction pattern indicated that the as-synthesized products were α-Fe_2O_3 with well-crystallized rhombohedral structure. The crystallite size of the α-Fe_2O_3 nanoparticles synthesized through citric acid and triethanolamine was 5 and 6 nm, respectively. SEM observation showed that the α-Fe_2O_3 products consist of spherical-like shape with uniform size distribution. The absorption edge of the α-Fe_2O_3 nanoparticles were measured at 558 and 563 nm. Optical measurement revealed that the band gap value of α-Fe_2O_3 nanoparticles was 2.22 and 2.20 eV. The photocatalytic activity of the α-Fe_2O_3 nanoparticles was analyzed by degradation of methylene orange, and the α-Fe_2O_3 nanoparticles showed excellent photocatalytic performance.

Graphical Abstract

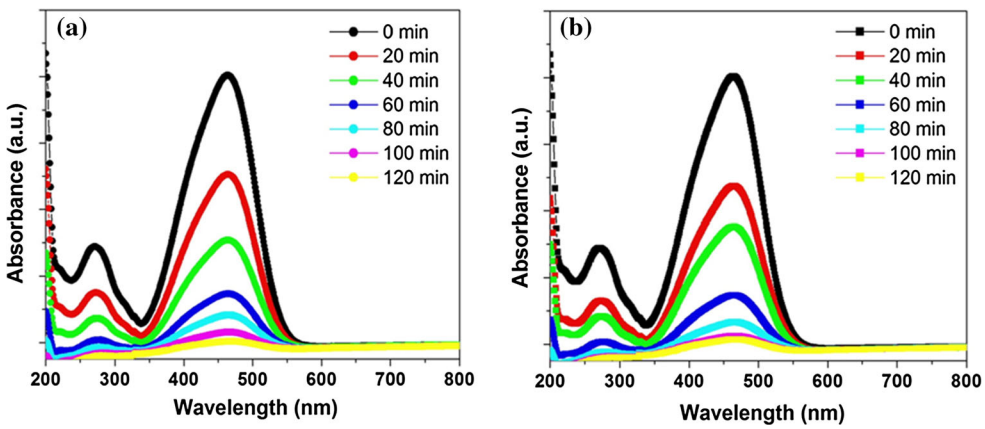

M. Alagiri (✉) · S. B. A. Hamid
Nanotechnology and Catalysis Research Centre (NANOCAT), University of Malaya, 50603 Kuala Lumpur, Malaysia
e-mail: smazhagiri@gmail.com

M. Alagiri
Center for Material Science and Nano Devices, Department of Physics, SRM University, Kattankulathur, Kancheepuram (D.t) 603203, Tamil Nadu, India

Keywords α-Fe_2O_3 nanoparticles · Sol–gel processes · Catalysis · Scanning electron microscopy · X-ray diffraction

1 Introduction

Recently, there is an increasing attention in the preparation of nanostructures owing to their excellent electronic, optical, magnetic, chemical, and thermal properties [1]. Currently, nanomagnetic materials have become much attention in materials science due to their potential applications in biotechnology, data storage, magnetic fluids, magnetic resonance imaging, biomedicine, biotechnology, and environmental remediation [2, 3]. In particular, iron oxide nanoparticles have various potential applications including contrast agent in magnetic resonance imaging, pigments, magnetic storage media, catalysts, chloroform sensors, and magnetic separation of photocatalytic nanoparticles [4, 5]. Depending on the iron oxidation state (Fe^{2+} or Fe^{3+}), iron oxide shows different crystal structures that consist of hematite (α-Fe_2O_3), maghemite (Fe_3O_4), and magnetite (γ-Fe_2O_3). Among these, hematite nanoparticles have paid significant attention from both theoretical and their potential applications in magnetic recording media, catalysis, pigments, lithium-ion batteries, anticorrosive agents, gas sensors, water treatment, and photocatalysis [6–12]. All these applications require that the nanoparticles are homogeneous in size, chemically stable, and well dispersed in liquid media. Hematite is an environment-friendly antiferromagnetic n-type semiconductor (E_g = 2.1 eV) and the most thermodynamically stable state of iron oxide at ambient temperature. Various methods exist for the preparation of α-Fe_2O_3 nanoparticles including magnetic sputtering [13], hydrothermal synthesis [14], sol–gel process [15], ultrasonic spray pyrolysis [16], electrochemical anodization [17], and vapor–solid growth techniques [18]. In this paper, we synthesized α-Fe_2O_3 nanostructures through two different sol–gel methods using citric acid and triethanolamine. The reasons for chosen sol–gel method are as follows: the sol–gel method does not require high pressure, the preparation of nanoparticles through the sol–gel method is very simple, it does not require any special equipment, and it is simple to obtain high-quality nanopowders of controlled structure, morphology, size, and homogeneous distribution. The reasons for choosing citric acid and triethanolamine as gelling agents are as follows: easily available chemicals, low-cost materials, and very easy to form a transparent gel with iron(III) nitrate nonahydrate. The main objective of the current paper is to study the morphology, structure, band gap, and the photocatalytic activity of the α-Fe_2O_3 nanoparticles.

2 Experiments

2.1 Preparation of α-Fe_2O_3 samples

The α-Fe_2O_3 nanoparticles were prepared through citric acid. In a typical experimental procedure, 1.5 g of iron(III) nitrate nonahydrate was dissolved in 60 ml of deionized water. Then 3 g of citric acid was added to the above solution, and the mixture was stirred for 2 h. The sodium hydroxide solution was added to the above mixed solution to adjust the pH value of 10. The mixture was allowed for magnetic stirring until the homogeneous solution was obtained. The homogeneous solution was continued to stirring and slow evaporation at 70 °C until a highly viscous residual was formed. After it was dried at 110 °C, a gel precursor was formed. To obtain α-Fe_2O_3 nanoparticles, the formed gel was calcined at 400 °C for 6 h. The synthesized sample is denoted by sample A.

The α-Fe_2O_3 nanoparticles were synthesized in the presence of triethanolamine. In the activating process, 1.5 g of iron(III) nitrate nonahydrate was dissolved in 60 ml of deionized water. Then 2 ml of triethanolamine was added to the above solution, and the mixture was stirred for 2 h. The sodium hydroxide solution was added to the above mixed solution to adjust the pH value of 10. The mixture was allowed for magnetic stirring until the transparent solution. The homogeneous solution was continued to stirring and slow evaporation at 70 °C until a highly viscous residual was formed. After it was dried at 110 °C, a gel precursor was formed. To obtain α-Fe_2O_3 nanoparticles, the formed gel was calcined at 400 °C for 6 h. The synthesized sample is denoted by sample B.

The X-ray powder diffraction pattern of the samples were carried out with a Bruker D8 advance X-ray diffractrometer using $CuK\alpha_1$ radiation (λ = 1.5406 Å), and the samples were scanned from 10° to 80° (2θ) with a scanning rate of 1° min^{-1}. Raman spectrum was recorded using a Renishaw InVia Laser Raman Microscope with a He–Ne laser. The surface morphology of synthesized materials were analyzed using scanning electron microscopy (SEM, model Oxford Instruments at an accelerating voltage of 10 kV). For SEM analysis, the powder samples were placed on conductive copper sticking tape. FTIR spectra were recorded from 400 to 4000 cm^{-1} with a Bruker IFS 66/S spectrometer using KBr pellet technique. Optical properties were measured using PerkinElmer lambda 35 UV–Visible spectrophotometer.

2.2 Photocatalytic activity

The photocatalytic activity of α-Fe_2O_3 nanoparticles were determined by measuring the degradation rate of MO, which is used here as a model pollutant. Methyl orange is an azo dye. This is a well-known acid–base indicator. For the photocatalytic degradation experiment, 0.2 g of α-Fe_2O_3 catalyst was dispersed in 10 mg/l of MO. To establish the adsorption/desorption equilibrium between

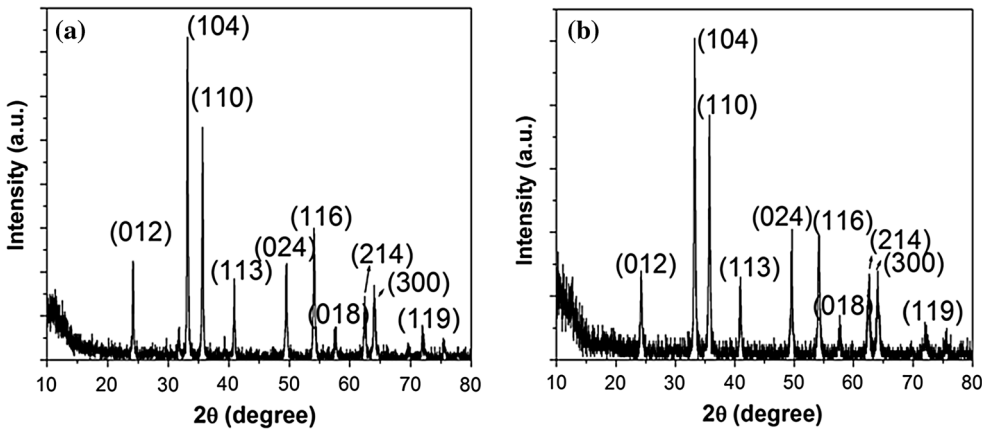

Fig. 1 XRD pattern of **a** sample A and **b** sample B

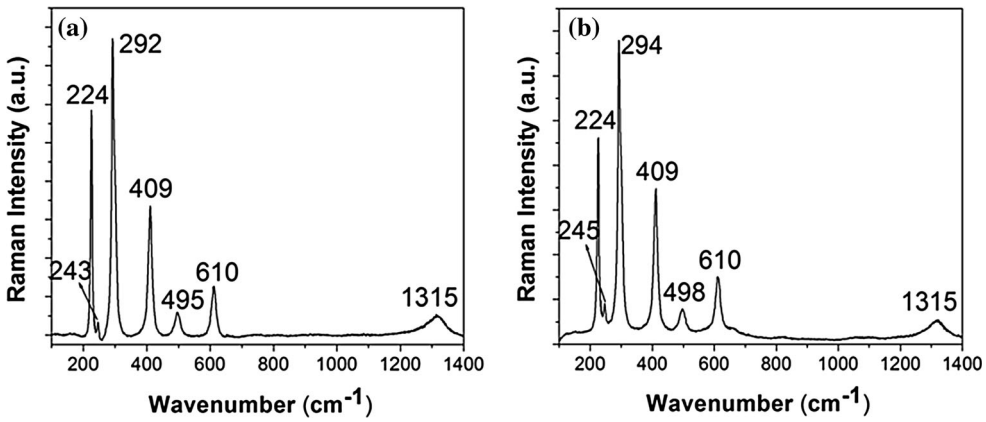

Fig. 2 Raman spectrum of **a** sample A and **b** sample B

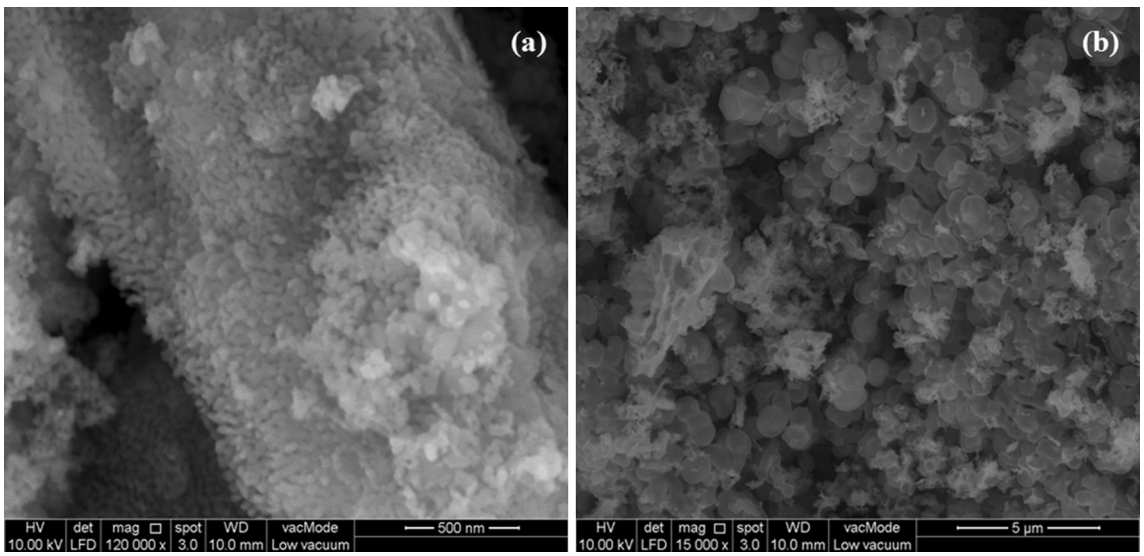

Fig. 3 SEM image of **a** sample A and **b** sample B

the MO molecules and the surface of the photocatalyst, the suspension was stirred in the dark for 40 min before turning on the lamps. During the illumination, 4 ml of suspension was taken out and centrifuged at 20 min time intervals. Then the MO concentration of clean solution was measured by a spectrometer.

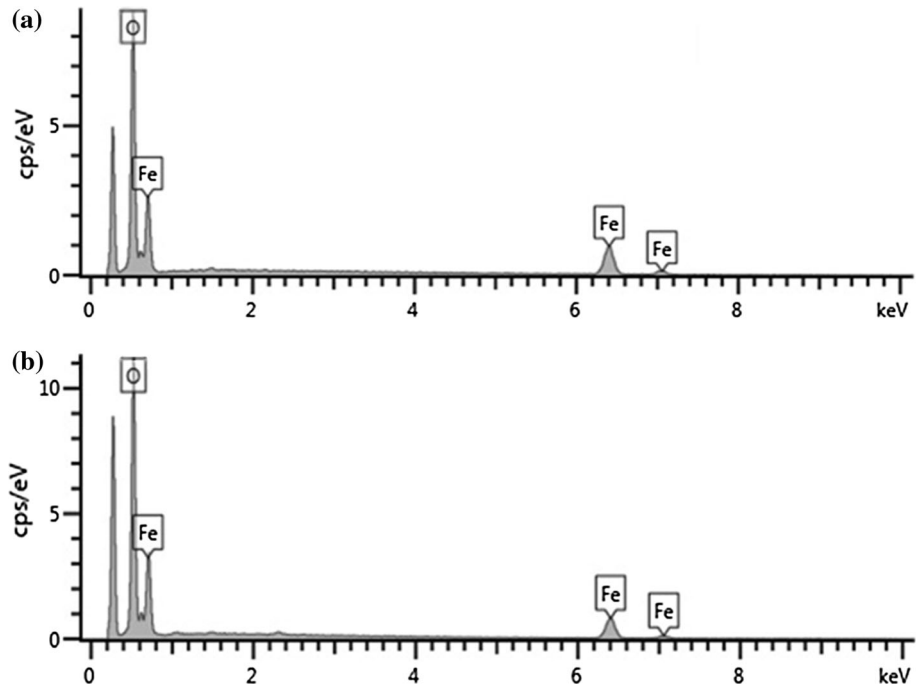

Fig. 4 EDX spectrum of **a** sample A and **b** sample B

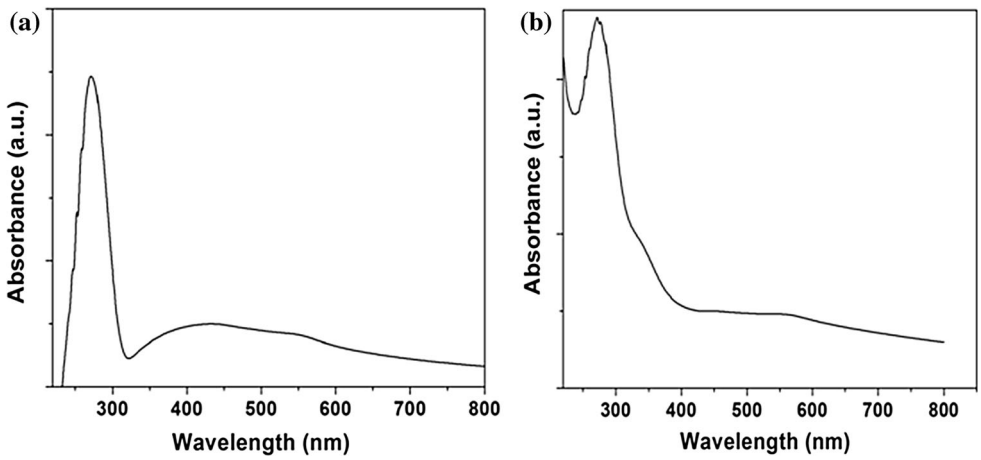

Fig. 5 UV-Visible spectrum of **a** sample A and **b** sample B

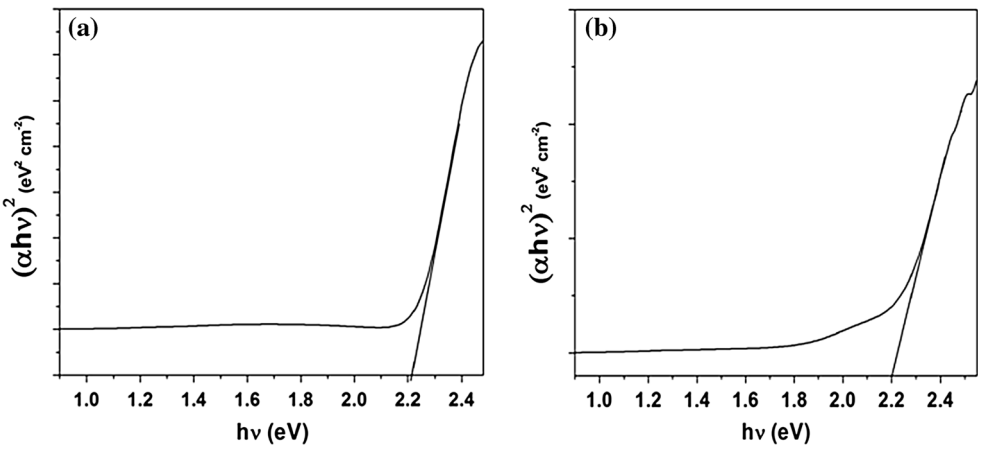

Fig. 6 Band gap plot [$h\nu$ vs. $(\alpha h\nu)^2$] of **a** sample A and **b** sample B

3 Results and discussion

3.1 XRD analysis

The chemical structure and crystallite size of the as-synthesized α-Fe_2O_3 nanoparticles were analyzed using a power XRD patterns. Figure 1a, b shows the XRD patterns of sample A and B. It was found that the prepared samples were crystalline and the XRD pattern has peaks at $2\theta = 24.13$, 33.15, 35.612, 40.85, 49.48, 54.09, 57.59, 62.41, 63.99, and 72.26, which assigned to (012), (104), (110), (113), (024), (116), (018), (214), (300), and (119) Bragg reflections of the rhombohedral phase (JCPDS card no: 33-0664) [19]; no other phases are detected. The lattice parameter values of the samples are: $a = b = 5.03560$ and $c = 13.74890$. The crystallite size was evaluated by Debye–Scherrer equation ($D = 0.89\ \lambda/(\beta \cos \theta)$, where, D, λ, θ, and β are, respectively, the average crystalline size of the particles, the wavelength of the X-rays, the Bragg angle, and the FWHM of a peak in radians). The crystallite size of sample A and B is 5 and 6 nm.

3.2 Raman analysis

The chemical compositions of the as-obtained samples were investigated by Raman spectrum analysis. Figure 2a, b illustrates the Raman spectrum of samples A and B. The Raman absorption peaks of sample A observed at 224, 243, 292, 409, 495, 610, and 1315 cm^{-1}. The Raman absorption peaks of sample B showed at 224, 245, 294, 409, 498, 610, and 1315 cm^{-1}, which corresponds to the characteristics of the α-Fe_2O_3 rhombohedral structure. This is in good agreement with the results of the XRD measurement. The positions of all the peaks are consistent with the result reported earlier [20, 21].

3.3 SEM images

In order to analyze the surface morphology and elemental composition of the synthesized samples, FESEM and EDX were carried out and shown in Figs. 3 and 4. The typical FESEM images of sample A and B are shown in Fig. 3a, b, and it is clearly found that the surface of α-Fe_2O_3 nanoparticles prepared by the sol–gel method is in spherical-like shape with uniform size distribution. Qualitative elemental composition was measured by the EDX spectra as shown in Fig. 4. The prepared samples composed of elemental iron and oxygen peaks only. No other peaks could be noticed, suggesting only pure crystalline α-Fe_2O_3 nanoparticles were formed.

3.4 Optical properties

UV–Vis spectra were used to measure the absorption edge of α-Fe_2O_3 nanoparticles. Figure 5 shows the UV–Vis absorption spectra of α-Fe_2O_3 nanoparticles. The absorption bands are observed at 558 and 272 nm for sample A, and the absorption bands are found at 563 and 272 nm for sample B. The absorption in the UV region corresponds to the direct charge transfer transitions of O^{2-} 2p → Fe^{3+} 3d, and the absorption in the visible region is due to the Fe^{3+} 3d → 3d indirect transition. The relationship between the absorption coefficient and the incident photon energy of semiconductors was given by the following equation [22]:

$$\alpha h\nu = \left(h\nu - E_g\right)^{1/2}$$

where 'α' is optical absorption coefficient, $h\nu$ is the photon energy, and E_g is the band gap energy for direct transitions. As shown in Fig. 6a, b, the band gap value of sample A and B was 2.22 and 2.20 eV, respectively. This value is consistent with those reported in the literature [23, 24].

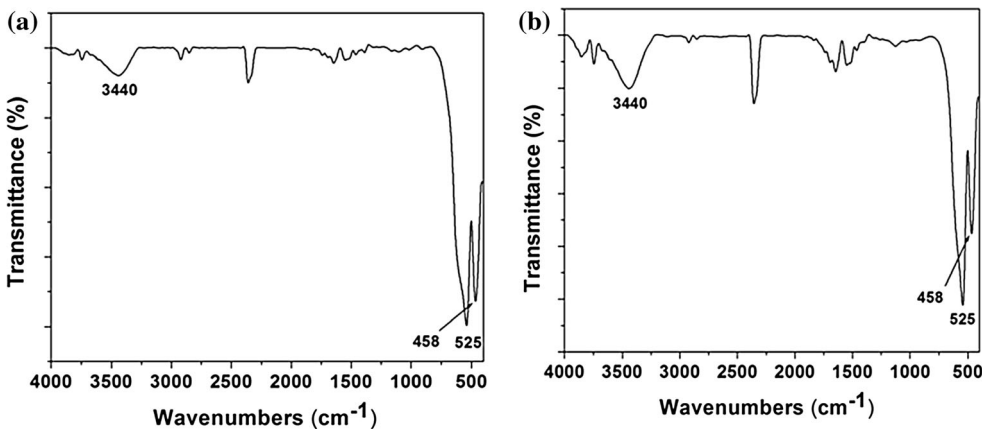

Fig. 7 FTIR spectra of **a** sample A and **b** sample B

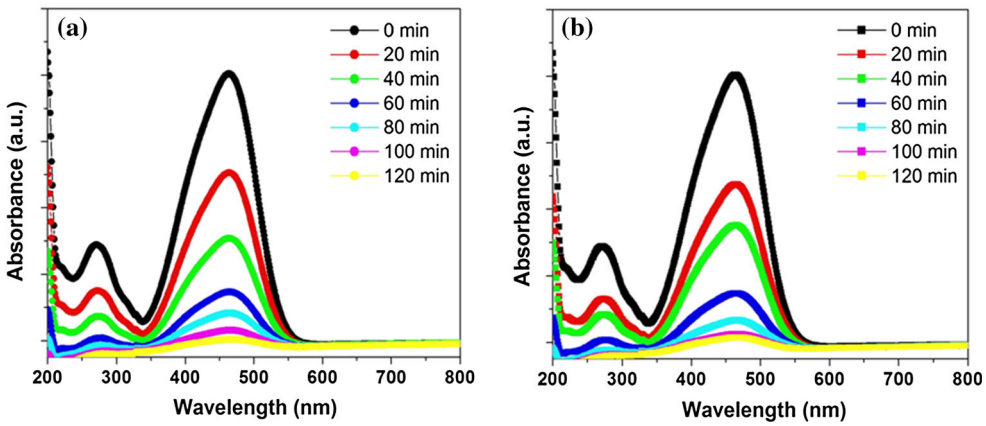

Fig. 8 UV–Vis spectroscopic changes of the MO solutions in the presence of α-Fe_2O_3 nanoparticles with variation of irradiation time of **a** sample A and **b** sample B

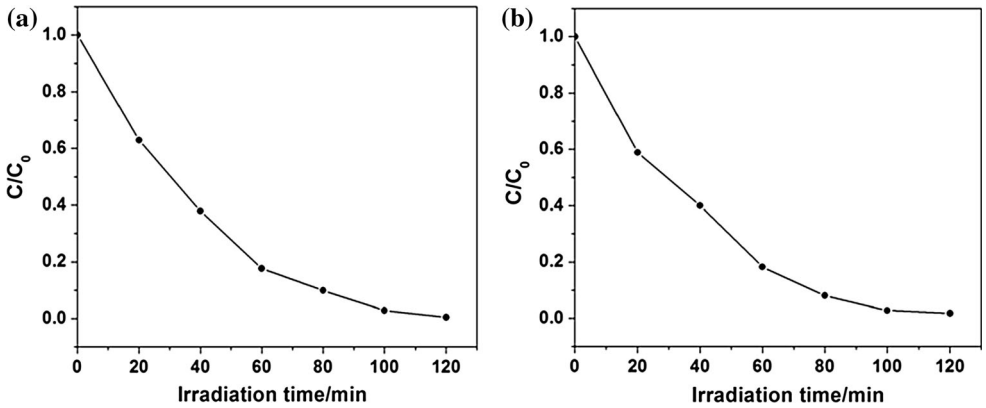

Fig. 9 Change of MO concentration as a function of irradiation time **a** sample A and **b** sample B (C_0 is the initial concentration and C is the concentration at any time)

3.5 FTIR analysis

FTIR analysis is used to find the chemical bonds present in the sample. Figure 7 shows the FTIR spectrum of the prepared samples A and B. The following band assignments were present in the synthesized samples: The band at 3440 cm^{-1} was attributed to the OH vibration, and the peaks at 458 and 525 cm^{-1} correspond to α-Fe_2O_3 band [25]. No other prominent FTIR bands related with citric acid and triethanolamine have been found in the FTIR spectrum, which suggests that the prepared samples are pure α-Fe_2O_3 nanostructure. This is in good agreement with the previous reports [23].

3.6 Photocatalytic activity of α-Fe_2O_3 samples

Photocatalytic decomposition of methyl orange was used to measure the photocatalytic behavior of the prepared α-Fe_2O_3 nanoparticles. The α-Fe_2O_3 nanoparticles showed a photocatalytic activity, and as shown in Fig. 8a, b, it can be observed clearly that the intensity of the peak decreased along with the illumination time. The optimum photocatalytic efficiency is observed at 120 min under irradiation [26]. Figure 9a, b illustrates the changes of the MO relative concentrations (C/C_0) as a function of irradiation time t, where C is the concentration of MO at the irradiation time t, and C_0 is the initial concentration. It can be clearly seen that the α-Fe_2O_3 samples exhibited visible-light photocatalytic properties in the degradation of MO.

4 Conclusion

Spherical-like α-Fe_2O_3 nanoparticles has been successfully developed by sol–gel method. XRD patterns showed that the as-synthesized sample was exactly α-Fe_2O_3 with rhombohedral structure. SEM results indicated that the as-prepared product composed of spherical-like shape with uniform size distribution. Optical studies showed that the band gap value of α-Fe_2O_3 nanoparticles was 2.22 and 2.20 eV.

Acknowledgments One of the authors M. Alagiri is thankful to the University of Malaya for providing research fellowship.

References

1. Xia Y, Yang P, Sun Y, Wu Y, Mayers B, Gates B, Yin Y, Kim F, Yan H (2003) Adv Mater 15:353
2. Gupta AK, Gupta M (2005) Biomaterials 26:3995
3. Lu AH, Salabas EL, Schuth F (2007) Angew Chem Int Ed 46:1222
4. Rahman MM, Jamal A, Khan SB, Faisal M (2011) Superlattices Microstruct 50:369
5. Patzke GR, Zhou Y, Kontic R, Conrad F (2010) Angew Chem Int Ed 49:2
6. Zhan SH, Chen DR, Jiao XL, Liu SS (2007) J Colliods Interface Sci 308:265
7. Chen J, Xu L, Li W, Gou X (2005) Adv Mater 17:582
8. Cao SW, Zhu YJ (2008) J Phys Chem C 112:6253
9. Zhang XL, Sui CH, Gong J, Su ZM, Qu LY (2007) J Phys Chem C 111:9049
10. Kamada K, Sohb N (2014) J Asian Ceram Soc. doi:10.1016/j.jascer.2014.10.004
11. Lu X, Chen L, Shi Y, Xu T, Liu M (2013) Matter lett 106:447
12. Li H, Zhao Z, Li X, Shi Y, Zhu Z, Tade M, Liu S (2012) Mater Res Bull 47:1459
13. Miller EL, Paluselli D, Marsen B, Rocheleau RE (2004) Thin Solid Films 466:307
14. Tang B, Wang G, Zhuo L, Ge J, Cui L (2006) Inorg Chem 45:5196
15. Wang X, Chen X, Gao L, Zheng H, Ji M, Tang C, Shen T, Zhang Z (2004) J Mater Chem 14:905
16. Cesar I, Kay A, Martinez JAG, Gratzel M (2006) J Am Chem Soc 128:4582
17. Prakasam HE, Varghese OK, Paulose M, Mor GK, Grimes CA (2006) Nanotechnology 17:4285
18. Fu YY, Wang RM, Xu J, Chen J, Yan Y, Narlikar AV, Zhang H (2003) Chem Phys Lett 79:373
19. Wanga F, Qin XF, Meng YF, Guo ZL, Yang LX, Ming YF (2013) Mater Sci Semicond Process 16:802
20. Rahman G, Joo OS (2013) Mater Chem Phys 140:316
21. Marinho JZ, Montes RHO, Moura AP, Longo E, Varela JA, Munoz RAA, Lima RC (2014) Mater Res Bull 49:572
22. Zhang Z, Hossain MF, Takahashi T (2010) Mater Lett 64:435
23. Shi JB, Lee CW, Guo JW, Cheng MJ, Wu C, Chen CJ et al (2007) Mater Lett 61:5268
24. Pandey BK, Shahi AK, Shah J, Kotnala RK, Gopal R (2014) Appl Surf Sci 289:462
25. Krehula S, Musi S (2007) J Alloys Compd 431:56
26. Cheng XL, Jiang JS, Jin CY, Lin CC, Zeng Y, Zhang QH (2014) Chem Eng J 236:139